The neutron transmission of natFe, 197Au and natW

Beyer, R.; Junghans, A. R.; Schillebeeckx, P.; Sirakov, I.; Song, T.-Y.; Bemmerer, D.; Capote, R.; Ferrari, A.; Hartmann, A.; Hannaske, R.; Heyse, J.; Kim, H. I.; Kim, J. W.; Kögler, T.; Lee, C. W.; Lee, Y.-O.; Massarczyk, R.; Müller, S. E.; Reinhardt, T. P.; Röder, M.; Schmidt, K.; Schwengner, R.; Szücs, T.; Takacs, M. P.; Wagner, A.; Wagner, L.; Yang, S.-C.;

Originally published:

May 2018

European Physical Journal A 54(2018), 81

DOI: https://doi.org/10.1140/epja/i2018-12505-7

Perma-Link to Publication Repository of HZDR:

https://www.hzdr.de/publications/Publ-26704

EPJ manuscript No.
(will be inserted by the editor)

The neutron transmission of ^{nat}Fe, ^{197}Au and ^{nat}W

Roland Beyer[1,a], Arnd R. Junghans[1], Peter Schillebeeckx[2], Ivan Sirakov[3], Tae-Yung Song[4], Daniel Bemmerer[1], Roberto Capote[5], Anna Ferrari[1], Andreas Hartmann[1], Roland Hannaske[1,6], Jan Heyse[2], Hyeon Il Kim[4], Jong Woon Kim[4], Toni Kögler[1,6], Cheol Woo Lee[4], Young-Ouk Lee[4], Ralph Massarczyk[1,6,b], Stefan E. Müller[1], Tobias P. Reinhardt[1,6], Marko Röder[1,6], Konrad Schmidt[1,6,c], Ronald Schwengner[1], Tamás Szücs[1], Marcell P. Takács[1,6], Andreas Wagner[1], Louis Wagner[1,6], and Sung-Chul Yang[4]

[1] Helmholtz-Zentrum Dresden - Rossendorf, Bautzner Landstr. 400, D-01328 Dresden, Germany
[2] European Commission Joint Research Centre - JRC Geel, Retieseweg 111, B-2440 Geel, Belgium
[3] Institute for Nuclear Research and Nuclear Energy, BAS, BG-1784 Sofia, Bulgaria
[4] Korea Atomic Energy Research Institute, P.O.Box 105, Yuseong, Daejeon, Korea
[5] Nuclear Data Section, International Atomic Energy Agency, PO Box 100, A-1400 Vienna, Austria
[6] Technische Universität Dresden, 01062 Dresden, Germany

Received: date / Revised version: date

Abstract. Neutron total cross sections of ^{nat}Fe, ^{197}Au and ^{nat}W have been measured at the *n*ELBE neutron time-of-flight facility in the energy range from 0.2 – 8 MeV with an uncertainty due to counting statistics of up to 2 % and a total uncertainty due to systematic effects of 1 %. The neutrons are produced with the superconducting electron accelerator ELBE using a liquid lead circuit as photo-neutron target. By periodical sample-in-sample-out measurements the transmission of the sample materials has been determined using a low-threshold plastic scintillation detector. The resulting effective total cross sections show good agreement with previously measured data that cover only part of the energy range available at *n*ELBE. The results have also been compared to evaluated library files and recent calculations based on a dispersive coupled channel optical model potential.

PACS. XX.XX.XX No PACS code given

1 Introduction

The neutron total cross section is the sum of the neutron induced partial cross sections for all open reaction channels, *e.g.* elastic and inelastic scattering, radiative capture, charged particle emission, neutron-induced fission, (n,xn) reactions. It can be measured in a transmission experiment, which allows a high precision of a few percent. Neutron total cross sections are an important experimental input for the evaluation of neutron-induced cross sections. The transmission determined from the count rates of the neutron beam transmitted through the sample relative to the count rate without sample is independent of the neutron detection efficiency, see *e.g.* refs. [1,2]. Neutron total cross sections show a large sensitivity to both compound nucleus model and optical model parameters in the fast-neutron energy range, where resonances in the cross sections overlap or cannot be resolved experimentally.

Dispersive coupled-channels calculations have improved the description of the total cross section experimental data for nuclides with various nuclear structures, *e.g.*, the soft-rotor coupling for even iron isotopes [3,4] and actinides [5], vibrational-rotational coupling for statically deformed nuclides like actinides [6] or rigid-rotor coupling for tungsten [7,8] and gold [8]. Optical model parameters are available from the RIPL-3 data base of IAEA [8]. For gold the nuclear data evaluation also profits from data in the unresolved resonance region, where statistical resonance parameters are used [9].

For many nuclides neutron total cross sections have been measured with high precision at Los Alamos National Laboratory [10] from 5 to 560 MeV. There is also an extensive set of measurements by Foster Jr. and Glasgow [11] from 2.5 up to 15 MeV. The measurements presented here will allow to extend the range from about 8 MeV down to 150 keV which covers the important first "Ramsauer" oscillation in the total cross section in the region of maximum relevance for fast reactors.

Iron as a major component in steel is an important structural material in many nuclear applications. It is also

[a] e-mail: roland.beyer@hzdr.de
[b] *Present address:* Los Alamos National Laboratory, Los Alamos, NM 87545, USA
[c] *Present address:* National Superconducting Cyclotron Laboratory, Michigan State University, East Lansing, MI 48824, USA

used in the cladding for fuel elements in sodium cooled reactors. Iron has been included in the list of isotopes for the international nuclear data evaluation project CIELO [12–14]. The major isotope of iron - ^{56}Fe - is a typical near-magic vibrational nucleus with low level density and a first excited one-phonon state around 850 keV. Therefore, resonant structures extend up to to several MeV excitation energy in the total cross section, and observed fluctuations have been incorporated into the evaluated data bases.

The total cross section of ^{197}Au is an item on the High Priority Request list of OECD/NEA [15] and gold is also an important neutron dosimeter [16,17]. Additionally, neutron capture on gold is a Neutron Standard reaction at the thermal energy, and from 200 keV up to 2.5 MeV [18,19].

Natural tungsten ^{nat}W is an important structural material to be used as plasma facing material in fusion reactors, it is also a component of reduced-activation ferritic-martensitic steels. An account of the total cross section of ^{nat}W measured at *n*ELBE has already been published in ref. [20].

2 The *n*ELBE time-of-flight facility

At the Helmholtz-Zentrum Dresden - Rossendorf (HZDR), Germany, the first photo-neutron source at a superconducting electron accelerator dedicated to measurements in the fast neutron range has been built. The facility has been upgraded with an enlarged time-of-flight experimental area, and a new compact liquid-lead circuit is utilized as a neutron-producing target [21,22]. A floorplan is shown in fig. 1. A flight path of about 5 to 9 m can be used for time-of-flight measurements. The room return of neutrons is reduced by locating all walls, ceiling and floor at least 3 m away from the neutron beam axis. The electron beam is accelerated to 30 MeV in continuous-wave mode by superconducting cavities. The maximum average beam current at a micro-pulse rate of 13 MHz is 1 mA. The accelerator produces high brilliance beams with variable micropulse repetition rates and duty cycles. The bunch duration is only about 5 ps, so that the time-of-flight resolution is not degraded and short flight paths can be used with a high-resolution detection system. The typical repetition rate for time-of-flight measurements is 100 to 400 kHz.

The neutron source strength at the nominal beam current has been calculated with the Monte Carlo N-Particle Transport Code MCNP-4C3 to be about 10^{13} neutrons/s [22]. The technical design including thermo-mechanical parameters of the liquid lead circuit and the beam dump is discussed in ref. [23]. The electron beam passes through a beryllium window mounted on a stainless-steel vacuum chamber and hits the neutron producing target, consisting of a molybdenum channel confining the liquid lead. The channel has a rhombic cross section with 11 mm side length. The electrons generate bremsstrahlung which releases neutrons in secondary (γ,n) reactions on lead. These leave the neutron producing target almost isotropically,

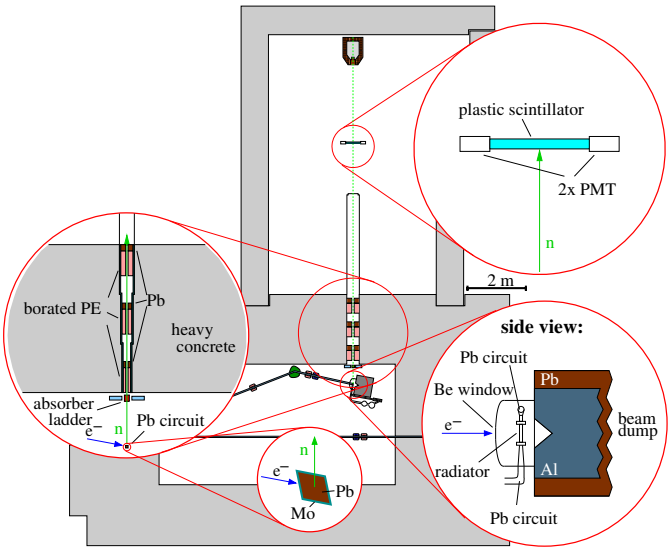

Fig. 1. Floor plan of the neutron time-of-flight facility *n*ELBE at HZDR, Dresden. The neutrons are produced by the electron beam hitting a liquid lead circuit as neutron producing target, see inset on the lower right. A neutron beam is shaped by a collimator and guided to the neutron time-of-flight hall, see inset on the left. The detection setup is located in the time-of-flight hall, see upper inset. For neutron transmission experiments a plastic scintillator with a low threshold for recoil proton signals is used. The transmission samples are located in a movable absorber ladder in the front of the collimator.

whereas the angular distributions of electrons and photons are strongly forward-peaked. The collimator axis is located at 100 degrees with respect to the electron beam direction. The properties of the collimator and the neutron beam at the experimental area have been optimized using MCNP-4C3 in order to maintain the correlation of time-of-flight and neutron energy [22]. The collimator of 2.5 m length contains three replaceable elements of lead and borated polyethylene that are mounted inside a precision steel tube.

3 Transmission experiment

The neutron transmission T is determined from the ratio of the background and deadtime corrected count rates R with sample in the beam to sample out of the beam as a function of neutron time-of-flight t:

$$T_{\mathrm{exp}} = \frac{R_{\mathrm{in}}}{R_{\mathrm{out}}} \qquad (1)$$

From the measured transmission as a function of time-of-flight $T_{\mathrm{exp}}(E_{\mathrm{n}}(t_{\mathrm{n}}))$ an effective neutron total cross section $\langle\sigma_{\mathrm{tot}}(E_{\mathrm{n}})\rangle$ can be determined:

$$\langle\sigma_{\mathrm{tot}}(E_{\mathrm{n}})\rangle = -\frac{1}{n}\ln T_{\mathrm{exp}} \qquad (2)$$

Different correction required in the resolved and the unresolved resonance range will be discussed in sec. 4.

Table 1. Fe, Au, W transmission sample properties. The iron conforms to ARMCO grade 4 99.9 %, the gold conforms to standard fine gold (99.99 %) and the tungsten has a purity of 99.95 %.

sample	mass (g)	diameter (mm)	areal density (atoms/barn)
Fe	77.275(1)	25.01(1)	0.16959(27)
Au	163.760(1)	26.01(1)	0.09422(14)
W	153.200(1)	25.29(1)	0.09990(16)

The samples and bremsstrahlung absorbers were right circular cylinders precisely machined. The areal density of the transmission samples n was determined from their masses with a digital analytic scale (KERN ABT 320-4M) and their diameters using a vernier micrometer screw (Tesamaster), see table 1. The length was 16 mm for the gold and the tungsten sample and 20 mm for the iron sample.

The samples together with bremsstrahlung absorbers were mounted in a motor-driven computer-controlled absorber ladder directly in front of the collimator entrance. The conical neutron-beam collimator has an entrance aperture diameter of 20 mm increasing to 30 mm at the exit. In this geometry small diameter samples were used with a typical neutron-transmission factor of about 0.5. The samples were periodically moved in and out of the beam to compensate for possible long-term drifts in the neutron beam intensity. The order of the cycle was ^{197}Au, ^{nat}W, ^{nat}Fe with an sample out setting following each sample. The data-taking time per cycle for the sample out setting was 600 s (reduced to 300 s for the second half of the experiment) and 1200 s for the ^{nat}Fe, ^{197}Au and ^{nat}W samples. The total measurement time was about 107 hours. Each sample position including the empty one was combined with a 3 cm thick Pb absorber to reduce the bremsstrahlung count rate. All Pb absorbers were made from the same technical lead alloy (PbSb4).

The transmitted neutrons were detected using a plastic scintillator (Eljen EJ-200, 200 mm × 42 mm × 11 mm) that was read out on both ends using high-gain Hamamatsu R2059-01 photomultiplier tubes (PMT). It was positioned at a flight path length of 852.1 cm. In this experiment the scintillator is surrounded by a 1 cm thick lead shield to reduce the room background count rate. The coincidence of the two PMT signals allows to detect also low energy proton recoils and to achieve a low neutron energy detection threshold [24]. A typical time-of-flight spectrum is shown in fig. 2. About 150 ns after the bremsstrahlung neutrons start to hit the detector. The time-of-flight resolution determined from the width of the bremsstrahlung peak is about Δt(FWHM) = 1.25 ns. The detection threshold for recoil protons in this detector is at about 10 keV [24]. The overlap neutron energy for the micropulse repetition rate (101.563 kHz) and flight path is 3.9 keV which is below the detection threshold of the detector.

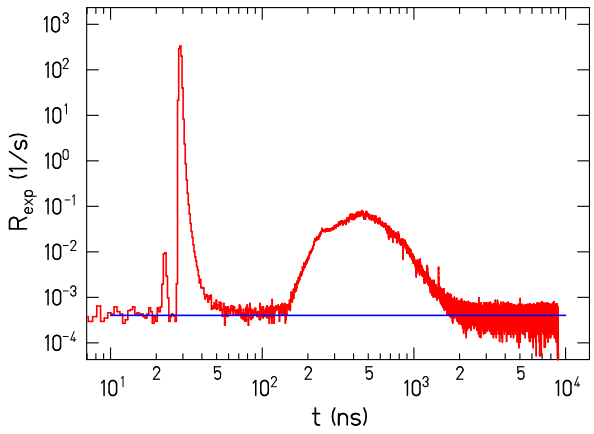

Fig. 2. Dead-time corrected time-of-flight spectrum with Au sample from a subset of the data taken (t_{real} = 37200 s). PMT after-pulses are suppressed as described in the text. A narrow condition on the time-difference of the PMT signals is used to suppress *e.g.* double hits. The first peak at 22 ns is due to double hits in the scintillator. The bremsstrahlung peak is located at 28.4 ns, its width is 1.25 ns (FWHM). The neutron time-of-flight range is from about 150 to 2500 ns. The blue line is the result of a fit of a constant time-independent background rate. The bin size of the spectrum is 0.5 ns.

The electron beam intensity was limited to the sub μA range to keep the detector count rate below 12.5 kHz (sample out setting). The count rates with sample were 3.0 kHz (Au), 3.2 kHz (W) and 6.6 kHz (Fe). This corresponds to a neutron count rate for the sample out setting of about 110 n/s. On average, only every eighth accelerator bunch is registered by the detector (either with a bremsstrahlung or neutron induced signal).

The time-of-flight of the transmitted neutrons was measured in list mode with the real-time data acquisition software package MBS (Multi-Branch-System) developed at GSI, Darmstadt. The data acquisition setup consists of a single VME/NIM crate with a CES RIO4 front-end processor using the real-time operating system Lynx OS. The schematic diagram is shown in fig. 3. The PMT signals and the accelerator frequency are fed into a CAEN V1290A multi-hit multi-event time-to-digital converter (TDC) with 25 ps least significant bit (LSB). This TDC is operated in trigger matching mode using a programmable time window with 13 μs width. The time-of-flight spectrum is determined from the coincident time-sum of both PMT signals relative to the accelerator frequency. A software condition is set on the time-difference of the two PMT signals to select events from the center of the beam spot on the scintillator.

A CAEN V965A charge-to-digital converter (QDC) is used to determine the charge of the PMT signals. The QDC buffer can hold 32 events while the TDC has a 32 KWords deep buffer. Therefore the latter can register many more events before it has to be readout. The QDC data are only used to monitor the threshold of the constant

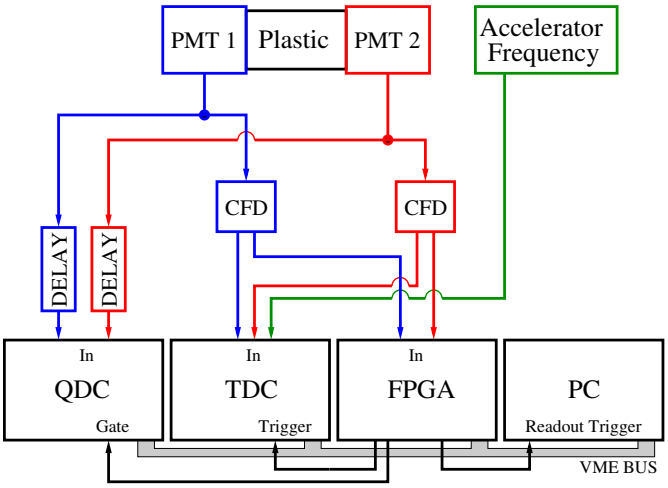

Fig. 3. Electronics-schematic of the transmission experiment. See text for details.

fraction discriminators (CFD) that are set just below the single photo-electron peaks of the PMTs. That means, a correlation between QDC and TDC data is not required, therefore the time when the QDC is busy or its memory full can be ignored and the readout frequency can be reduced. A readout trigger is produced typically after 700 event triggers. Furthermore, the TDC is not stopped during readout but continues measuring. By this modification the dead time can be minimized. This is an improvement compared to a former experiment described in ref. [25]. *E.g.*, the live time for sample out setting measurements is increased from 56 % to 95 % (see also sec. 4.2).

The transmission measurement requires a high level of after-pulse rejection due to the nature of the photo-neutron source, as the instantaneous intensity of the bremsstrahlung is more than four orders of magnitude higher than the neutron intensity, see fig. 2. The random background rate is dominated to 80 to 90 % by the beam-off background.

The PMTs having a high gain ($2 \cdot 10^7$) cause after-pulses to occur in a time range from 100 ns to several microseconds after a real pulse. The ELBE accelerator period used in this measurement is 9.8 μs. The relevant neutron time of flight range is about 200 ns to 2.5 μs. This implies that after-pulses from the bremsstrahlung occur in this range. They are frequent enough to cause random coincidences in the readout of the two PMTs. In order to suppress triggering on after-pulses, the FPGA trigger logic was programmed to have a 3 μs dead time after each coincidence. In this way effectively all after-pulses from the gamma-flash in the neutron time-of-flight region are suppressed. This is a further improvement to our former experiment [25] where the 3 μs dead time was created by gate and delay generators after the CFDs which caused additional dead time due to the higher singles rates of the PMTs. In this experiment neutron time-of-flight signals are only registered during accelerator periods where the bremsstrahlung was not registered before in the same accelerator period.

4 Data analysis and experimental uncertainties

To determine the neutron transmission and the total cross section from the measured time-of-flight distribution with a relative accuracy of a few percent several corrections are in order:

1. Correction for a time-of-flight dependent dead time
2. Subtraction of a random background in the time-of-flight spectra
3. Correction for fluctuations of the neutron-beam intensity
4. Correction for in-scattering of neutrons
5. Correction for resonant self-shielding in thick transmission samples

These corrections to our transmission experiment have already been discussed in ref. [25]. In this section the important corrections will be briefly revisited and the effect of resonant self-shielding in the unresolved resonance region (URR) will be discussed.

Random background and dead-time corrections are important. The fluctuations of the neutron-beam intensity were measured during the sample cycling and found to have a small influence, see the discussion in [25]. In-scattering of neutrons was minimized by the geometry of the setup: The collimator strongly limits the solid angle under which neutrons can be registered and only neutrons passing through the full length of the sample can hit the detector. The probability for multiple in-scattering of fast neutrons has been found to be less than 0.1 % [25].

4.1 Random background correction

In neutron sources using moderators to slow down the neutrons this background can be time-of-flight dependent and must be determined in separate measurements, see [1]. In this transmission experiment a low beam intensity and a very compact neutron producing target without any materials that would slow down neutrons were used. The random background can be described by a constant value in time-of-flight. It is mostly dominated by random coincidences due to ambient natural radioactivity whereas the room return background of neutrons is rather low [25]. Fig. 2 shows a typical background rate from a fit to the time-of-flight region below the neutron detection threshold of the detector.

4.2 Dead time correction

As the photo-neutron source in this experiment is pulsed with a repetition rate of 101.563 kHz, the dead-time correction is not constant but time-of-flight dependent. The time-of-flight dependent dead-time correction $\alpha(t_{\mathrm{ToF}}) = t_{\mathrm{live}}/t_{\mathrm{real}}$ is determined in the same way as described in refs. [25,26]. The dead time per event is measured with a 40 MHz clock by the trigger logic implemented in the FPGA module. For each event the starting time-of-flight

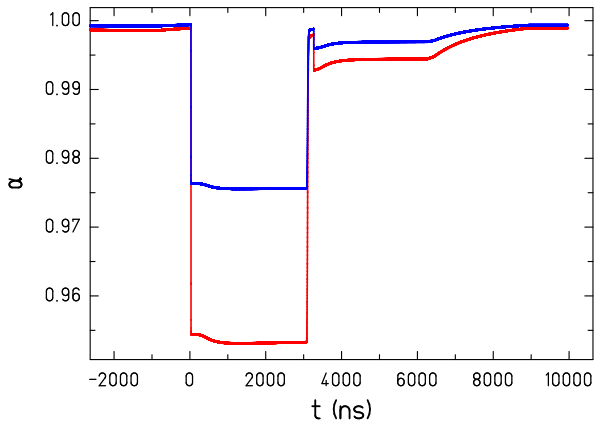

Fig. 4. Time-of-flight dependent dead-time correction factor $\alpha = t_{\rm live}/t_{\rm real}$. The dead-time correction increases with the arrival of bremsstrahlung radiation at $t = 28.4$ ns. The neutron intensity, being much lower, only causes a small change in α in the neutron time of flight range. The blue curve shows the dead-time correction for the iron sample measurement; the red curve for sample out setting.

channel and the length of the dead time are known. In the offline data analysis a histogram is filled containing the information on how often each time-of-flight channel was blocked. Most of the dead time is due to bremsstrahlung signals causing a 3 μs long step in time-of-flight dependent dead-time correction factor, see fig. 4. The dead time caused by neutron induced signals starts later and is much shorter.

In this experiment the dead time due to the duration of the CFD signals of the single PMTs is negligible as their width is reduced to 20 ns. To improve the suppression of after-pulses in the list-mode data analysis a filter has been applied. If a coincidence event of the two PMTs occurs within the length of the programmable time window (here up to 9.5 μs before the triggering event), it is discarded as a potential after-pulse. This is essentially the length of the accelerator period. If the time interval is increased to *e.g.* 12.5 μs this filter starts to eliminate real pulses and not only after-pulses from the time-of-flight spectrum leading to a loss of counts. Therefore, the time window has to be short enough to prevent extension into the previous accelerator period.

4.3 Resonant self-shielding

Resonant self-shielding can be an important correction at low neutron energy, where the total cross section can have strong, separated compound-nuclear resonances [27]. If there are sharp resonances in the total cross section the experimental resolution can become insufficient to completely resolve them. Then the cross section calculated with the experimental transmission according to eq. (2) will differ from the real total cross section. This is the case for the ^{nat}Fe cross section reported here and also for the low energy part below about 250 keV of ^{197}Au and ^{nat}W.

In the URR resonant self-shielding still can play a role in transmission measurements [1,9,28]. The magnitude of the effect depends on sample thickness and the average resonance width and spacing. The resonant self-shielding effect in the URR can be calculated using data tables of cross sections in MCNP including the probability-table method [29,30]. The correction for the resonant self absorption in the URR can be calculated according to:

$$T_{\rm sim}(E_{\rm n}) = F_{\rm T} \exp\{-n\langle\sigma_{\rm tot}\rangle\} \qquad (3)$$

where the correction factor $F_{\rm T}$ is deduced from the leftmost equation in

$$F_{\rm T} = \frac{T_{\rm sim}(E_{\rm n})}{\exp\{-n\langle\sigma_{\rm tot}\rangle\}} \approx 1 + \frac{n^2}{2}{\rm var}(\sigma_{\rm tot}) \pm ... \qquad (4)$$

where $T_{\rm sim}(E_{\rm n})$ is the simulated neutron transmission taking into account resonant self-shielding in the unresolved resonance with the probability-table method in MCNP and $\exp\{-n\langle\sigma_{\rm tot}\rangle\}$ is the simulated neutron transmission with MCNP where only the average point-wise cross-section data are used without the probability-table method. The resulting transmission correction factors $F_{\rm T}$ due to the effect of resonant self-shielding in the ^{197}Au and the ^{nat}W sample are shown in fig. 5. The data tables currently included in MCNP contain unresolved resonance parameters only up to a neutron energy of 100 keV. To estimate the correction in the energy range covered by the present measurement a smoothed extrapolation of the simulated $F_{\rm T}$ has been done (see fig. 5) which might be indicative of its real continuing decrease. From this extrapolation it can be estimated that the correction would be below 1 % above 150 keV for both samples. However, this correction is not applied to the data presented here.

4.4 Unresolved resonant structures

Due to the high level density of the heavy deformed nuclei ^{197}Au and ^{nat}W the transmission data do not show significant resonant structures in the neutron energy range above 150 keV. The neutron resonance level spacing of the near-magic iron however is three orders of magnitude higher than in tungsten or gold. The measured transmission of ^{nat}Fe is shown in fig. 6. It is compared to the calculated transmissions $T_{\rm res}$ with and without taking an experimental resolution function $R(E_{\rm n} - E)$ (see *e.g.* [1,25]) into account via the relation:

$$T_{\rm res}(E_{\rm n}) = \int R(E_{\rm n} - E) \exp\{-n\sigma_{\rm tot}(E)\}\, {\rm d}E \qquad (5)$$

The measured transmission of ^{nat}Fe shows the effects of unresolved resonances leading to an experimental total cross section, that is not straightforward to be used in *e.g.* R-Matrix analysis of data. The s-wave resonances and their interference with potential scattering are well resolved. The much narrower resonant structure of $l > 0$

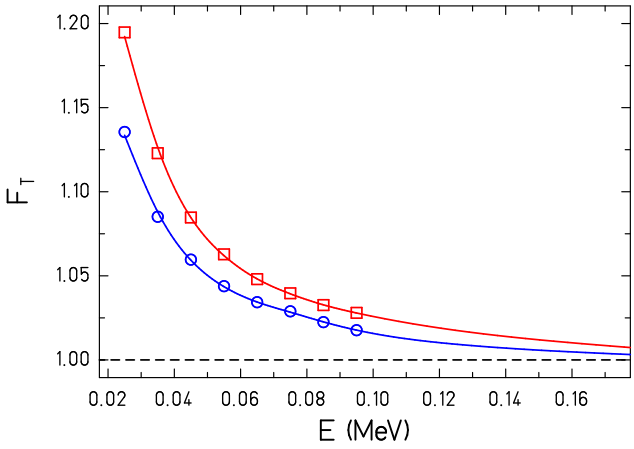

Fig. 5. The transmission correction factor F_T *vs.* neutron energy E calculated with MCNP for the ^{197}Au (blue circles) and the ^{nat}W (red squares) sample. Due to the resonant self-shielding in the URR the experimental transmission is larger than can be estimated based on the average point-wise total cross section. An MCNP calculation above 100 keV is not possible, as the required URR parameters do not exist in the available data files. The solid lines show smoothed extrapolations of the MCNP simulated correction factors F_T into the energy range covered by the present measurement.

resonances visible in the evaluated data based on experiments using a much longer flight path with a higher experimental resolution, *e.g.*, [31–34], is not resolved here. Frequent minima of the total cross section lead to a rather high transmission, that would require a thicker sample to be measured, whereas the sharp $l > 0$ resonances having a high peak will saturate and require a smaller sample thickness. The experimental resolution function of the *n*ELBE setup can be well described by a straightforward Gaussian resolution function using the time-of-flight resolution determined from the width Δt of the bremsstrahlung peak and the flight path variation ΔL due to thickness of neutron detector and the neutron producing target. However, the comparison of measured data with optical model cross sections, that describe the energy-averaged excitation function, is still possible.

5 Results

The neutron total cross sections of ^{nat}Fe, ^{197}Au and ^{nat}W have been measured in the energy range from about 0.15 to 8 MeV. The energy resolution $\Delta E/E$ increases in this energy range from $4 \cdot 10^{-3}$ to $1.2 \cdot 10^{-2}$ (FWHM). At energies above 2 MeV the energy resolution has been found to deteriorate due to scattering of neutrons in the lead shield of the plastic scintillator [25]. In this work the length of the scintillator has been reduced from 100 cm to 20 cm which should help to reduce this effect. This resolution is sufficient for average cross sections that can be compared with optical model calculations. Fig. 6 shows the measured transmission on iron of this work in comparison with the transmission calculated using the evaluated

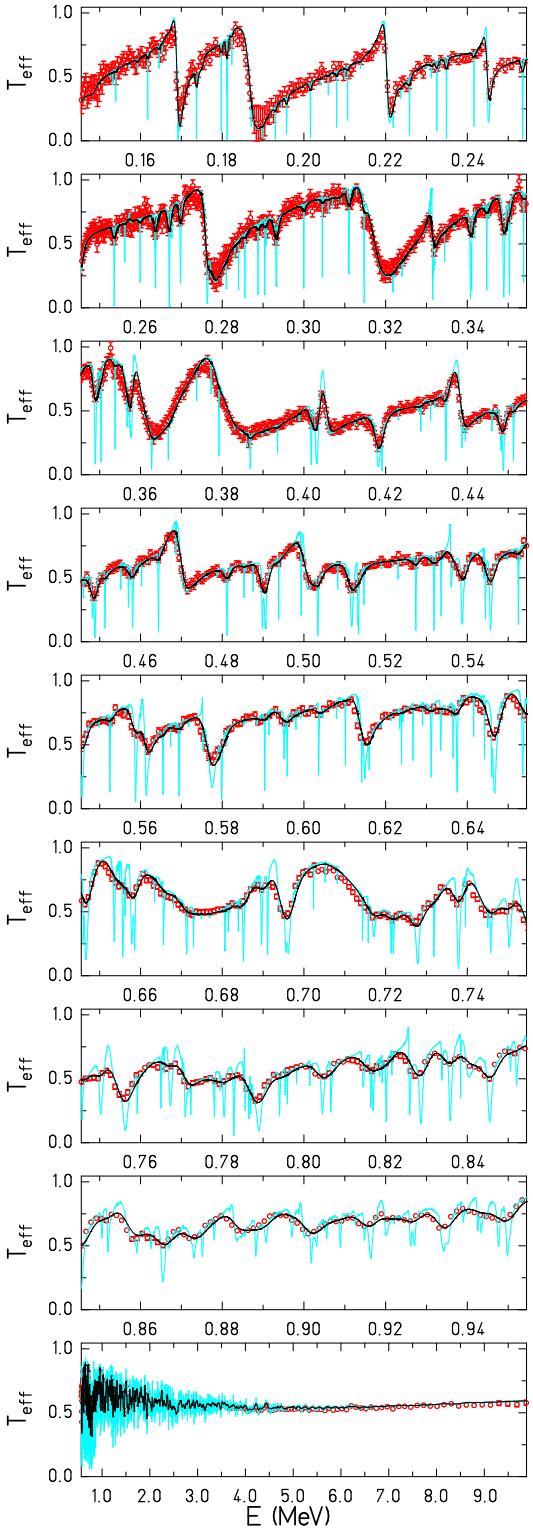

Fig. 6. Transmission of ^{nat}Fe measured in this work shown as red data circles (with 0.5 ns binning). The calculated transmission based on the evaluated cross section (JEFF-3.2=JEFF-3.1 [32]) of ^{nat}Fe is shown in cyan. The simulated transmission taking into account the experimental resolution function with eq. (5) using $\Delta t = 1.25$ ns (FWHM) and $\Delta L = 1.48$ cm (FWHM) is shown as a black curve.

cross section from JEFF-3.2 (=JEFF-3.1 [32]) which is based on a combination of data involving also the high-resolution measurement described in ref. [35] and older average cross section analyses. Fig. 7 shows the experimental cross section without a correction for resonant self-shielding. A good agreement is found with all measurements shown. Due to the short flight path this work does not have the time resolution to resolve narrow resonances in iron, only the broader s-wave resonances and interferences with potential scattering are resolved. However, a broad energy range from 0.15 to 8 MeV is covered allowing a comparison of the normalization of the higher resolution measurements that covered only smaller energy intervals. A connection to the precise measurements from Abfalterer *et al.* [10] that extend from a neutron energy of 5 MeV to several hundred MeV neutron energy is made.

In fig. 7 the total cross section of iron is also compared with predictions based on a recent dispersive-coupled-channels optical model (DCCOM) [3,4]. The model calculations were done for the iron isotopes ^{54,56,57,58}Fe and the total cross section for the natural isotopic composition was calculated from these isotopic data. The DCCOM results agree well with the total cross section above 4 MeV, at lower energies the resonant structure in the cross section cannot be described by the model, nor the minimum of the measured averaged cross section at 1 MeV. This behaviour is well known for near magic nuclei of the iron group, and the description of the observed reduction in the averaged total cross section requires l-dependent optical model potentials [36].

In fig. 8 the measured total cross section of ^{197}Au is shown in comparison with results from four high precision experiments [10,11,27,37]. The absolute agreement is very good and the precise data from Abfalterer *et al.* [10] are extended over the first single particle resonance down to 150 keV. In this energy range up to now only measurements using quasi-monoenergetic neutron beams were available. These data points are by about 2 % lower than the results reported in ref. [25] which suffered from a much higher dead time correction mentioned above. The results from Poenitz *et al.* [37] in this energy range are systematically higher and have larger uncertainties in the energy range from 0.5 to 1 MeV. Below 500 keV and above 1.5 MeV the deviation is smaller than 1 %. Below 800 keV the present data lie in between the JEFF-3.2 evaluation and the DCCOM prediction [4].

In fig. 9 the measured total cross section of ^{nat}W is shown in comparison with other experimental results [10, 11,27,37]. The data presented here agree very well with the high precision data from Abfalterer *et al.* [10] and extend down to 150 keV bridging some gaps in the data around 2 MeV and below 1 MeV. The agreement with the JEFF-3.2 evaluation [38] is poor, especially near the Ramsauer maximum. The ENDF/B-VII.1 evaluated data [39] based on the Trkov evaluation [7,40] is in good agreement with our measurements. Experimental total cross sections for ^{182,184,186}W with an uncertainty due to systematic effects of about 2 to 3 % do exist from measurements with isotopically enriched samples [41,42].

In figs. 7-9 only uncertainties due to counting statistics are plotted. They are in the order of 1 % to 8 % over the energy range from 0.2 to 8.0 MeV using a time-of-flight binsize of 2 ns corresponding to an energy binsize of 0.6 to 150 keV in that energy range. Using a binsize of 10 ns (*i.e.*, 3 to 764 keV) the uncertainties due to counting statistics can be reduced below 2 % over the complete energy range. The total uncertainty due to systematic effects is about 1 % including sample dimension, dead time correction, and background subtraction.

Acknowledgement

We thank the ELBE accelerator crew for providing very stable beam operation.

This work was supported by the German Federal Ministry for Education and Science (TRAKULA project, contract number 02NUK13A) and by the European Commission within the Seventh Framework Programme through Fission-2013-CHANDA (project number 605203).

References

1. P. Schillebeeckx, B. Becker, Y. Danon, K. Guber, H. Harada, J. Heyse, A.R. Junghans, S. Kopecky, C. Massimi, M.C. Moxon, N. Otuka, I. Sirakov, and K. Volev. Determination of resonance parameters and their covariances from neutron induced reaction cross section data. *Nucl. Data Sheets*, 113, 2012.
2. D.W. Miller. Neutron total cross section measurements. In J.B. Marion and J.L. Fowler, editors, *Fast Neutron Physics*, volume II, chapter V.A. Interscience Publishers John Wiley & Sons, 1963.
3. Rui Li, Weili Sun, E.Sh. Soukhovitskii, J.M. Quesada, and R. Capote. Dispersive coupled-channels optical-model potential with soft-rotator couplings for Cr, Fe, and Ni isotopes. *Phys. Rev. C*, 87:054611, 2013.
4. W. Sun, R. Lui, E.Sh. Soukhovitskii, J.M. Quesada, and R. Capote. A fully lane-consistent dispersive optical model potential for even Fe isotopes based on a soft-rotator model. *Nucl. Data Sheets*, 118:191–194, Apr 2014.
5. D. Martyanov, E.S. Soukhovitskii, R. Capote, J.M. Quesada, and S. Chiba. Optical model with multiple band couplings using soft rotator structure. volume 146, page 12031, 2017.
6. E.Sh. Soukhovitski, R. Capote, J.M. Quesada, S. Chiba, and D.S. Martyanov. Nucleon scattering on actinides using a dispersive optical model with extended couplings. *Phys. Rev. C*, 94:064605, Dec 2016.
7. A. Trkov, R. Capote, Kodeli I., and L. Leal. Evaluation of tungsten nuclear reaction data with covariances. *Nucl. Data Sheets*, 109:2905–2909, 2008. See evaluated data files and comments at http://www-nds.iaea.org/wolfram/.
8. R. Capote, M. Herman, P. Oblozinsky, P.C. Young, S. Goriely, T. Belgya, A.V. Ignatyuk, A.J. Koning, S. Hilaire, V.A. Plujko, M. Avrigeanu, O. Bersillon, M.B. Chadwick, T. Fukahori, Zhigang Ge, Yinlu Han, S. Kailas, J. Kopecky, V.M. Maslov, G. Reffo, M. Sin, E.Sh. Soukhovitskii, and P. Talou. RIPL - Reference Input Parameter Library for calculation of nuclear reactions and nuclear data evaluations. *Nucl. Data Sheets*, 110, 2009.

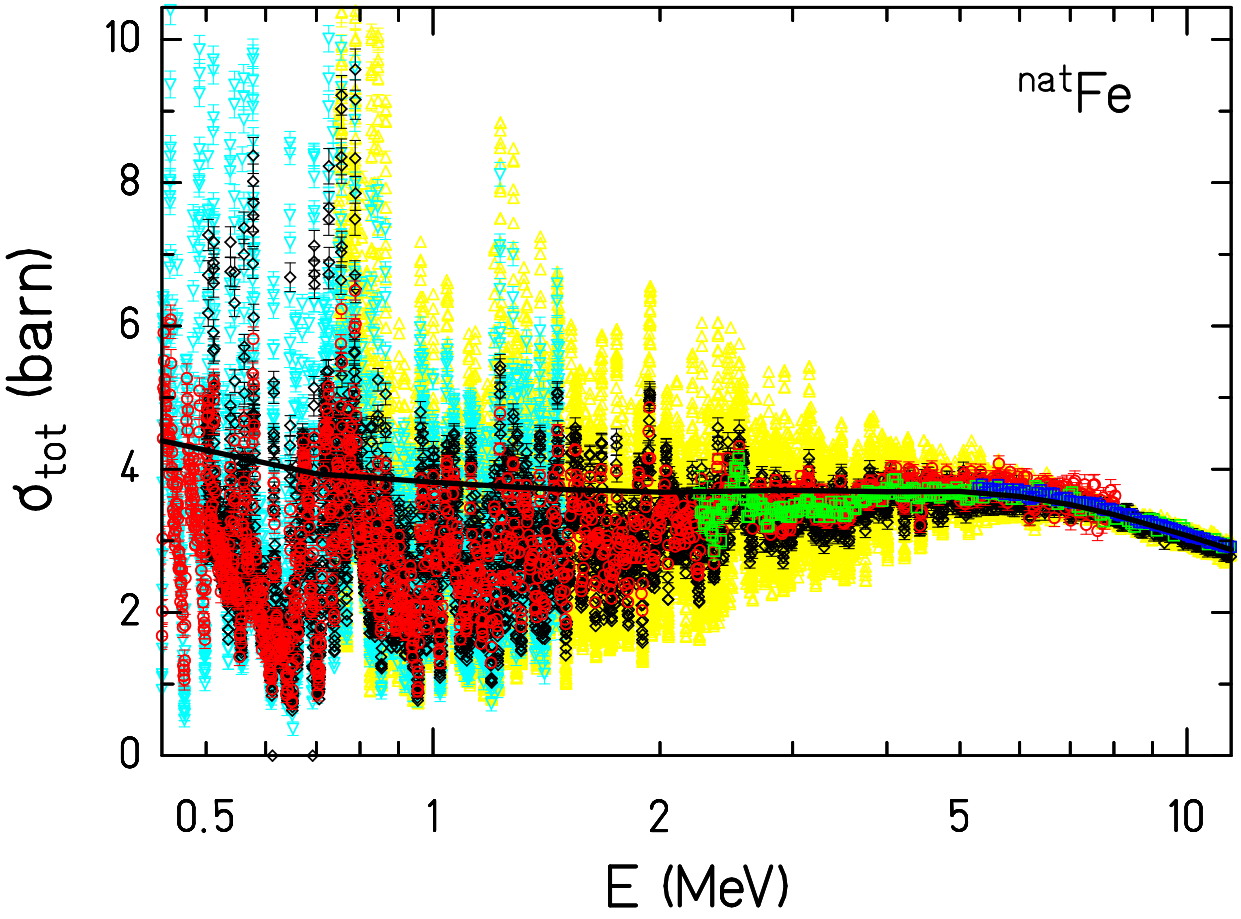

Fig. 7. Total neutron cross section of ^{nat}Fe in the energy range above 0.5 MeV measured in this work shown as red data circles. For comparison experimental cross sections measured at Oak Ridge [33] (cyan triangles down), at Karlsruhe [34] (black diamonds), Geel [35] (yellow triangles up), at Pacific Northwest Laboratories [11] (green squares) and Los Alamos [10] (blue squares) are plotted. The black line shows an optical model result from ref. [4].

9. I. Sirakov, B. Becker, R. Capote, E. Dupont, S. Kopecky, C. Massimi, and P. Schillebeeckx. Results of total cross section measurements for ^{197}Au in the neutron energy region from 4 to 108 keV at GELINA. *Eur. Phys. J. A*, 49:144, 2013.
10. W.P. Abfalterer, F.B. Bateman, F.S. Dietrich, R.W. Finlay, R.C. Haight, and G.L. Morgan. Measurement of neutron total cross sections up to 560 MeV. *Phys. Rev. C*, 63:044608, Mar 2001.
11. D.G. Foster Jr. and D.W. Glasgow. Neutron total cross sections, 2.5 - 15 MeV. i. experimental. *Phys. Rev. C*, 3:576, 1971.
12. OECD, Nuclear Energy Agency, WPEC Subgroup 40 (SG40). Collaborative international evaluated library organisation (CIELO) pilot project. https://www.oecd-nea.org/science/wpec/sg40-cielo/.
13. M. B. Chadwick, E. Dupont, E. Bauge, et al. The CIELO collaboration: Neutron reactions on ^{1}H, ^{16}O, ^{56}Fe, ^{235,238}U, and ^{239}Pu. *Nucl. Data Sheets*, 118:1–25, 2014.
14. M. B. Chadwick, R. Capote, A. Trkov, et al. CIELO Collaboration summary results: International evaluations of neutron reactions on uranium, plutonium, iron, oxygen and hydrogen. *Nucl. Data Sheets*, 148:xx, 2018.
15. OECD/NEA Nuclear Data High Priority Request List. https://www.oecd-nea.org/dbdata/hprl/.
16. E.M. Zsolnay, R. Capote, H. Nolthenius, and A. Trkov. Summary description of the new international reactor dosimetry and fusion file (IRDFF release 1.0). Technical Report INDC(NDS)-0616, IAEA, Vienna, 2012.
17. R. Capote, K.I. Zolotarev, V.G. Pronyaev, and A. Trkov. Updating and extending the IRDF-2002 dosimetry library. *J. of ASTM Internat.*, 9:JAI104119, 2012.
18. A.D. Carlson, V.G. Pronyaev, D.L. Smith, et al. International evaluation of neutron cross section standards. *Nucl. Data Sheets*, 110:3215–3324, 2009.
19. A.D. Carlson, V.G. Pronyaev, R. Capote, et al. Evaluation of neutron data standards. *Nucl. Data Sheets*, 148:xx, 2018.
20. T.-Y. Song, J.W. Kim, H.I. Kim, S.-C. Yang, C.W. Lee, Y.-O. Lee, A.R. Junghans, R. Beyer, T. Kögler,

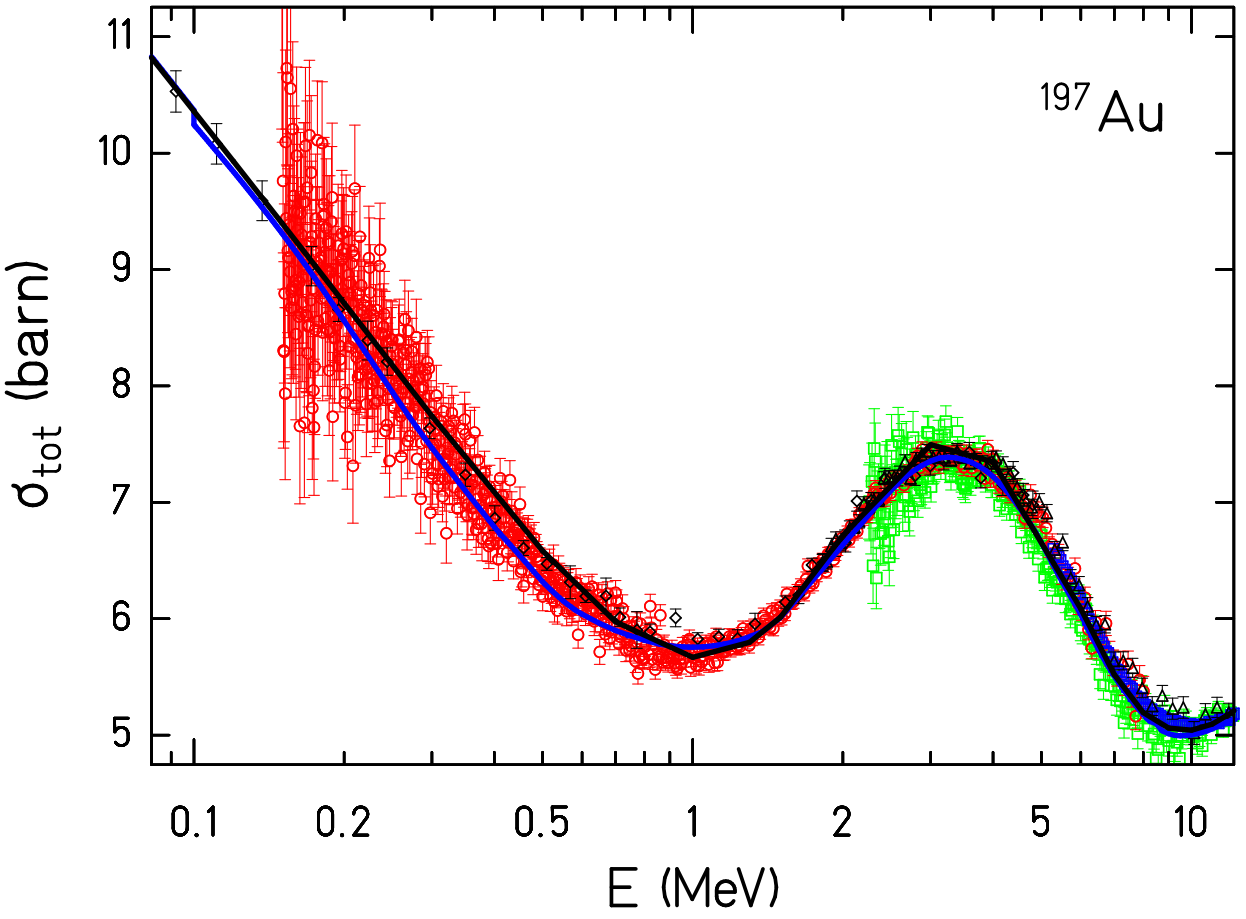

Fig. 8. Total neutron cross section of ^{197}Au measured in this work shown as red data circles (with 2 ns binning). For comparison experimental cross sections measured at the Argonne Fast Neutron Generator [27,37] (black diamonds and triangles), at Pacific Northwest Laboratories [11] (green squares) and at Los Alamos [10] (blue squares) are plotted. The black line shows an optical model result from ref. [8]. The blue line corresponds to the cross section from the JEFF-3.2 evaluated data library [38]. The evaluated cross section from ENDF/B-VII.1 [39] is identical to the data from JEFF-3.2.

R. Schwengner, R. Hannaske, L. Wagner, T.P. Reinhardt, M.P. Takács, R. Massarczyk, S. Müller, A. Ferrari, K. Schmidt, M. Röder, D. Bemmerer, T. Szücs, and A. Wagner. Neutron transmission measurement for natural W at nELBE. In *EPJ Web of Conferences*, volume 146, page 11044, 2017.

21. A.R. Junghans, R. Beyer, Z. Elekes, E. Grosse, R. Hannaske, T. Kögler, R. Massarczyk, R. Schwengner, and A. Wagner. Fast-neutron induced reactions at the nELBE time-of-flight facility. *Nucl. Data Sheets*, 119:349–352, May 2014.
22. J. Klug, E. Altstadt, C. Beckert, R. Beyer, H. Freiesleben, V. Galindo, E. Grosse, A.R. Junghans, D. Legrady, B. Naumann, K. Noack, G. Rusev, K.D. Schilling, R. Schlenk, S. Schneider, A. Wagner, and F.-P. Weiss. Development of a neutron time-of-flight source at the ELBE accelerator. *Nucl. Instr. Meth. A*, 577(3):641–653, JUL 2007.
23. E. Altstadt, C. Beckert, H. Freiesleben, V. Galindo, E. Grosse, A.R. Junghans, J. Klug, B. Naumann, S. Schneider, R. Schlenk, A. Wagner, and F-P. Weiss. A photo-neutron source for time-of-flight measurements at the radiation source ELBE. *Ann. Nucl. Energy*, 34(1-2):36–50, Jan 2007.
24. R. Beyer, E. Grosse, K. Heidel, J. Hutsch, A.R. Junghans, J. Klug, D. Legrady, R. Nolte, S. Roettger, M. Sobiella, and A. Wagner. Proton-recoil detectors for time-of-flight measurements of neutrons with kinetic energies from some tens of keV to a few MeV. *Nucl. Instr. Meth. A*, 575(3):449–455, Jun 2007.
25. R. Hannaske, Z. Elekes, R. Beyer, A.R. Junghans, D. Bemmerer, E. Birgersson, A. Ferrari, E. Grosse, M. Kempe, T. Kögler, M. Marta, R. Massarczyk, A. Matic, G. Schramm, R. Schwengner, and A. Wagner. Neutron total cross section measurements of gold and tantalum at the nELBE photoneutron source. *Eur. Phys. J. A*, 49(11):137, 2013.
26. R. Beyer, E. Birgersson, Z. Elekes, A. Ferrari, E. Grosse, R. Hannaske, A.R. Junghans, T. Kögler, R. Massarczyk, A. Matic, R. Nolte, R. Schwengner, and A. Wagner. Char-

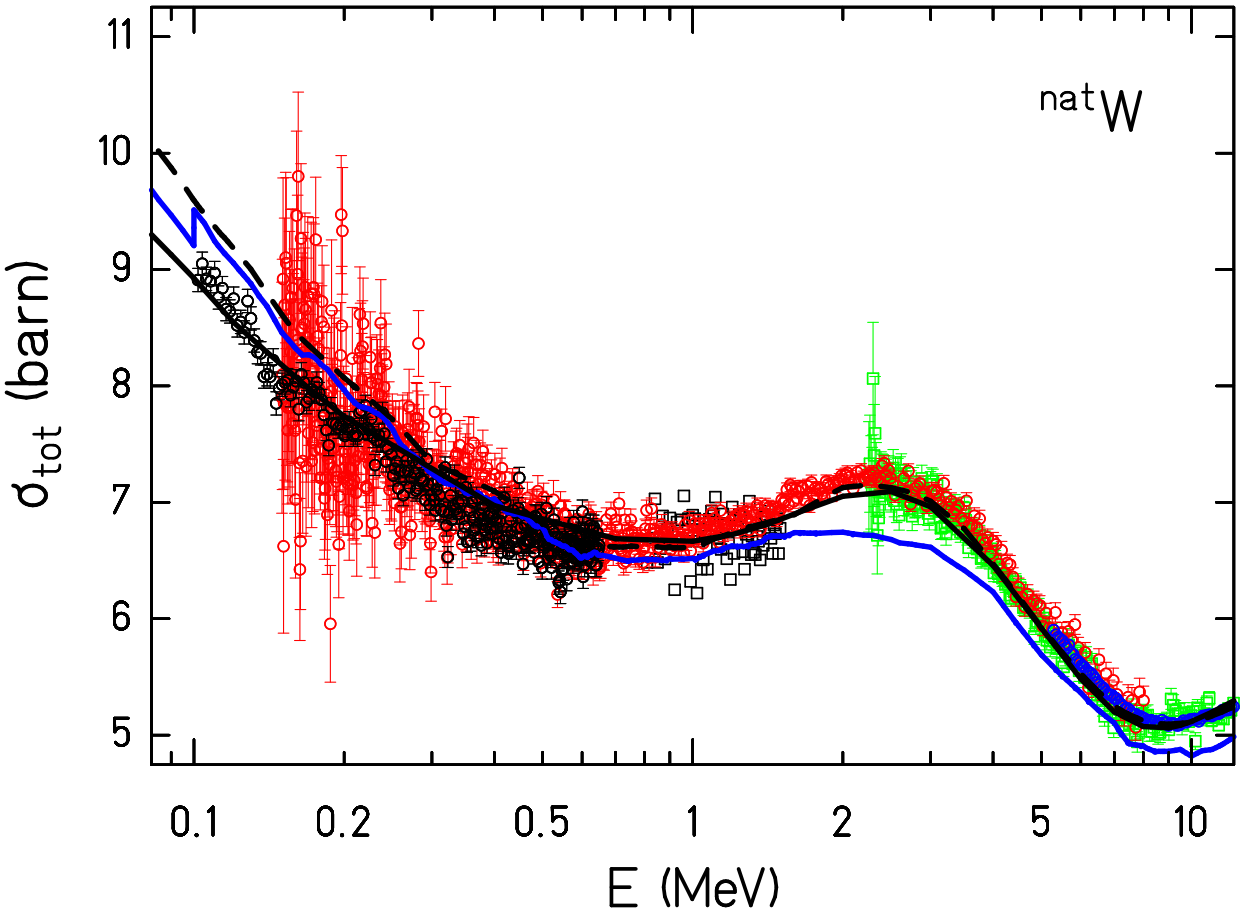

Fig. 9. Total neutron cross section of ^{nat}W measured in this work shown as red data circles (with 2 ns binning). For comparison experimental cross sections measured at the Argonne Fast Neutron Generator [43,44] (black circles and squares), at Pacific Northwest Laboratories [11] (green squares) and Los Alamos [10] (blue circles). The black line shows an optical model result for the natural isotopic composition of tungsten based on isotopic data from ref. [8]. The blue line corresponds to the cross section for the natural isotopic composition based on isotopic data from the JEFF-3.2 evaluated data library [38]. The dashed line shows the evaluated cross section from ENDF/B-VII.1 [39].

acterization of the neutron beam at nELBE. *Nucl. Instr. Meth. A*, 723:151–162, SEP 21 2013.

27. W.P. Poenitz, J.F. Whalen, and A.B. Smith. Total neutron cross sections of heavy nuclei. *Nucl. Sci. Eng.*, 78:333–341, 1981.
28. F.H. Fröhner. Evaluation and analysis of nuclear resonance data. Technical Report JEFF Report 18, OECD/NEA, 2000.
29. Leo B. Levitt. The probability table method for treating unresolved neutron resonances in Monte Carlo calculations. *Nucl. Sci. Eng.*, 49:450–457, 1972.
30. R.E. MacFarlane and A.C. Kahler. Methods for processing ENDF/B-VII with NJOY. *Nucl. Data Sheets*, 111:2739–2890, 2010.
31. A.J. Koning, H. Gruppelaar, and A. Hogenbirk. The EFF-3.0 evaluation for ^{56}Fe. *Fusion Eng. Des.*, 37:211–216, 1997.
32. A. Trkov, S. Masetti, M. Herman, A. Koning, H. Gruppelaar, A. Hogenbirk, S. Tagesen, H. Vonach, V.G. Pronyaev, and F. Froehner. Evaluation of neutron induced reactions on iron. CNDN-ENEA, 1998. Distributed as JEFF-3.1.
33. M.S. Pandey, J.B. Garg, J.A. Harvey, and W.M. Good. High resolution total neutron cross-section in ^{54}Fe and ^{56}Fe. In R.A. Schrack and C.D. Bowman, editors, *Proc. of Conf. on Nucl. Cross Sections and Tech. Volume II, Washington, D.C. March 3-7, 1975*, pages 748–753. National Bureau of Standards Special Publications 425, 1975.
34. S. Cierjacks, G. Schmalz, R. Töpke, R.R. Spencer, and F. Voss. Thick sample transmission measurement and resonance analysis of the total neutron cross section of iron. In R.A. Schrack and C.D. Bowman, editors, *Proc. of Conf. on Nucl. Cross Sections and Tech. Volume II, Washington, D.C. March 3-7, 1975*, pages 754–757. National Bureau of Standards Special Publications 425, 1975.
35. K. Berthold, C. Nazareth, G. Rohr, and H. Weigmann. High-resolution transmission data from geel. EXFOR data base entry 22276, 1995.

36. T. Kawano and F.H. Fröhner. Partial-wave analysis with the optical model for the resolved and unresolved resonance regions of ^{56}Fe. *Nucl. Sci. Eng.*, 127:130–138, 1997.
37. W.P. Poenitz and J.F. Whalen. Neutron total cross section measurements in the energy region from 47 keV to 20 MeV. Report ANL-NDM-80, Argonne National Laboratory, 1984.
38. JEFF Scientific Working group, Nuclear Energy Agency Data Bank. Joint evaluated fission and fusion file (jeff) release 3.2. OECD, 2014.
39. M. B. Chadwick, M. W. Herman, P. Obložinský, et al. ENDF/B-VII.1 nuclear data for science and technology: cross sections, covariances, fission product yields and decay data. *Nucl. Data Sheets*, 112:2887–2996, 2011.
40. A. Trkov, R. Capote, E.Sh. Soukhovitskii, L.C. Leal, M. Sin, I. Kodeli, and D.W. Muir. Covariances of evaluated nuclear cross section data for ^{232}Th, ^{180,182,183,184,186}W and ^{55}Mn. *Nucl. Data Sheets*, 112(12):3098 – 3119, 2011.
41. F.S. Dietrich, J.D. Anderson, R.W. Bauer, S.M. Grimes, R.W. Finlay, W.P. Abfalterer, F.B. Bateman, R.C. Haight, G.L. Morgan, E. Bauge, J.-P. Delaroche, and P. Romain. Importance of isovector effects in reproducing neutron total cross section differences in the W isotopes. *Phys. Rev. C*, 67:044606, Apr 2003.
42. P.T. Guenther, A.B. Smith, and J.F. Whalen. Fast-neutron total and scattering cross sections of ^{182}W, ^{184}W, and ^{186}W. *Phys. Rev. C*, 26(6):2433, 1982.
43. J.F. Whalen and J.W. Meadows. Fast neutron total cross sections using a mono-energetic source and an automated facility. Report ANL-7210, Argonne National Laboratory, 1966.
44. J.F. Whalen, R. Roge, and A.B. Smith. Fast-neutron total cross sections with an automated facility. In *Bulletin of the American Physical Society*, volume 9, page 651(Q13), 1964.